RSC Advances

PAPER

View Article Online
View Journal | View Issue

Cite this: *RSC Adv.*, 2025, **15**, 35532

A novel strategy for nephritis-associated infections: dual-antibacterial/anti-inflammatory effects of Schiff base

Yu Zhang, * Weiwei Fu and Xiangli Xue

Received 25th July 2025
Accepted 14th September 2025

DOI: 10.1039/d5ra05377c

rsc.li/rsc-advances

To address the antimicrobial treatment needs for lupus nephritis and pyelonephritis, this study designed and synthesized ten Schiff base derivatives using 4-(diethylamino)salicylaldehyde as the core scaffold *via* aldehyde-amine condensation reactions. Activity screening identified compound **D5** as exhibiting potent antibacterial activity against *Staphylococcus aureus* ATCC 29213 with an MIC of 8 μg mL^{-1}, demonstrating low cytotoxicity toward mammalian cells (HK-2, LO2) and no hemolysis at 256 μg mL^{-1}. Mechanistic studies revealed that **D5** disrupts bacterial membrane integrity, causing leakage of intracellular proteins and DNA. Furthermore, it completely eradicated bacteria within 10 hours at 8 × MIC concentration with a low propensity for resistance induction, and possessed both inhibitory and eradicative effects against biofilms. In an LPS-induced RAW 264.7 macrophage model, **D5** significantly downregulated the levels of inflammatory factors including TNF-α, IL-6, IL-1β, and NO. Preliminary druggability assessment confirmed its compliance with Lipinski's rule of five. In summary, **D5** combines potent antibacterial, anti-biofilm, and anti-inflammatory activities with an excellent safety profile, positioning it as a promising candidate compound for further development.

1. Introduction

The kidneys, as vital organs for human metabolism and excretion, have functional integrity that is directly linked to overall health. However, they are also frequent targets for severe infections and autoimmune diseases, with renal abscess and lupus nephritis (LN) representing two highly clinically challenging conditions characterized by high incidence, severe harm, and significant therapeutic complexities and limitations.[1–4] Renal abscesses are typically caused by bacterial infections, and *Staphylococcus aureus*, particularly methicillin-resistant *Staphylococcus aureus* (MRSA), is one of the key pathogens responsible for severe renal abscesses (such as renal carbuncle and perinephric abscess).[5] These infections often originate from hematogenous spread or ascending urinary tract infections, where bacteria colonize and proliferate within the renal parenchyma, triggering intense inflammatory reactions that lead to localized pus accumulation. Abscess formation disrupts normal renal tissue structure, resulting in progressive renal function impairment.[6,7] Current standard treatment primarily relies on conventional antibiotics (such as **Vancomycin** and linezolid for MRSA). However, antibiotic therapy faces multiple severe challenges: first, the increasingly prominent issue of drug resistance, where the widespread prevalence of highly resistant strains like MRSA diminishes the efficacy of conventional antibiotics, increasing the risk of treatment failure and potentially leading to disseminated infection and sepsis;[8] second, the barrier to drug penetration, where the low pH, hypoxic environment within renal abscesses, and the physical barrier of the abscess wall severely impede effective antibiotic penetration, making it difficult to achieve bactericidal concentrations at the site;[9] third, the formation of biofilms, where bacteria within abscesses readily form biofilms, significantly enhancing their resistance to both antibiotics and host immune defenses;[10] fourth, the insufficiency of mere bactericidal action in resolving inflammatory damage, as antibiotics, while killing bacteria, offer limited control over the ensuing "cytokine storm" (*e.g.*, massive release of inflammatory factors like TNF-α, IL-1β, IL-6) triggered by bacterial death.[11] This uncontrolled inflammatory response itself causes severe renal parenchymal damage and fibrosis. Consequently, the pathological progression of both renal abscesses (characterized by intense inflammation triggered by bacterial infection) and lupus nephritis (characterized by autoimmune-driven inflammation, often complicated by infection) intertwines the two core issues of infection and inflammation.[12] Existing single-target antibiotic therapies often address one aspect at the expense of the other. Therefore, developing novel dual-functional molecules that combine potent antibacterial activity (especially against common resistant pathogens like *S. aureus*) with strong anti-inflammatory effects holds extremely urgent clinical need and significant practical importance. This approach is critical for breaking the cycle of "inadequate

The Second Hospital of Qinhuangdao, Qinhuangdao, 066000, China. E-mail: 19316050110@163.com

bacterial clearance and uncontrolled inflammation" in renal abscess treatment and resolving the dilemma in LN management of "suppressing autoimmunity while potentially exacerbating infection risks."

Facing these complex clinical challenges, medicinal chemists have turned their attention to the historically significant yet rejuvenated structural scaffold—Schiff bases, compounds containing an imine group (–RC═N–).[13] Schiff bases represent an attractive platform for discovering novel antibacterial and anti-inflammatory lead compounds due to their relatively straightforward synthesis, rich structural modifiability, and increasingly demonstrated diverse biological activities. The antibacterial mechanisms of Schiff bases are relatively well-studied and characterized by multiple targets: (1) metal ion chelation, where the imine nitrogen and adjacent heteroatoms (*e.g.*, phenolic oxygen, heterocyclic nitrogen) effectively chelate metal ions essential for microbial growth (*e.g.*, Fe^{3+}, Zn^{2+}, Cu^{2+}), disrupting the function of metabolic enzymes (*e.g.*, respiratory chain enzymes, DNA synthesis enzymes);[14] (2) membrane disruption, where certain hydrophobic Schiff bases can insert into bacterial cell membranes, compromising integrity and increasing permeability, leading to content leakage;[15] (3) inhibition of virulence factors, with some Schiff bases reported to inhibit biofilm formation, quorum sensing, or toxin secretion.[16] Notably, extensive research confirms that Schiff bases formed from electron-rich aromatic aldehydes containing hydroxyl or amino groups (such as salicylaldehyde and its derivatives) often exhibit excellent activity against Gram-positive bacteria, particularly *Staphylococcus aureus* (including MRSA).[17] Therefore, designing novel Schiff bases based on the salicylaldehyde scaffold is a crucial strategy for developing new drugs against *S. aureus*, especially resistant strains. Recent years have also seen significant progress in research on the anti-inflammatory activity of Schiff base compounds, with mechanisms primarily focusing on regulating key inflammatory factors: they inhibit the phosphorylation-dependent degradation of IκBα, preventing NF-κB nuclear translocation, thereby downregulating the expression of critical pro-inflammatory mediators such as TNF-α, IL-6, IL-1β, COX-2, and iNOS.[18]

Salicylaldehyde derivatives themselves, such as the classic aspirin metabolite salicylic acid, have a long history of anti-inflammatory applications. Upon Schiff base formation, their molecular structures undergo significant changes, potentially optimizing or conferring new characteristics in lipophilicity, electron distribution, spatial conformation, and target-binding capabilities, which may lead to enhanced or novel anti-inflammatory activity compared to the parent salicylaldehyde or the corresponding amines.[19] 4-(diethylamino)salicylaldehyde, as an important derivative within the salicylaldehyde family, possesses unique structural advantages conferred by its features: the *para*-position diethylamino group is a strong electron-donating group, significantly enhancing the acidity of the ortho phenolic hydroxyl group and the electron density of the benzene ring; the phenolic hydroxyl group may form an intramolecular hydrogen bond with the adjacent aldehyde group or the resulting imine group, helping stabilize specific molecular conformations; the introduction of the diethylamino group modulates the molecule's lipophilicity (log *P*), improving its cell membrane permeability and tissue distribution – crucial for drug delivery to renal lesions (*e.g.*, renal parenchyma, glomeruli).[20–22] Although 4-(diethylamino)salicylaldehyde and its derivatives have found applications in fields like materials science, systematically designing and synthesizing Schiff bases using it as the core scaffold, deeply investigating their dual antibacterial and anti-inflammatory activities, and applying them to complex renal diseases like renal abscess and lupus nephritis – which simultaneously require control of both infection and inflammation – represents a frontier area of exploration with vast uncharted space and immense innovative potential.

Motivated by the aforementioned severe clinical challenges and the promising drug chemistry platform (Schiff bases, particularly the dual antibacterial and anti-inflammatory potential demonstrated by 4-(diethylamino)salicylaldehyde derivatives), this study was initiated. Utilizing 4-(diethylamino) salicylaldehyde as the core electronic scaffold and pharmacophore carrier, leveraging its capacity for intramolecular hydrogen bonding, the altered electronic properties conferred

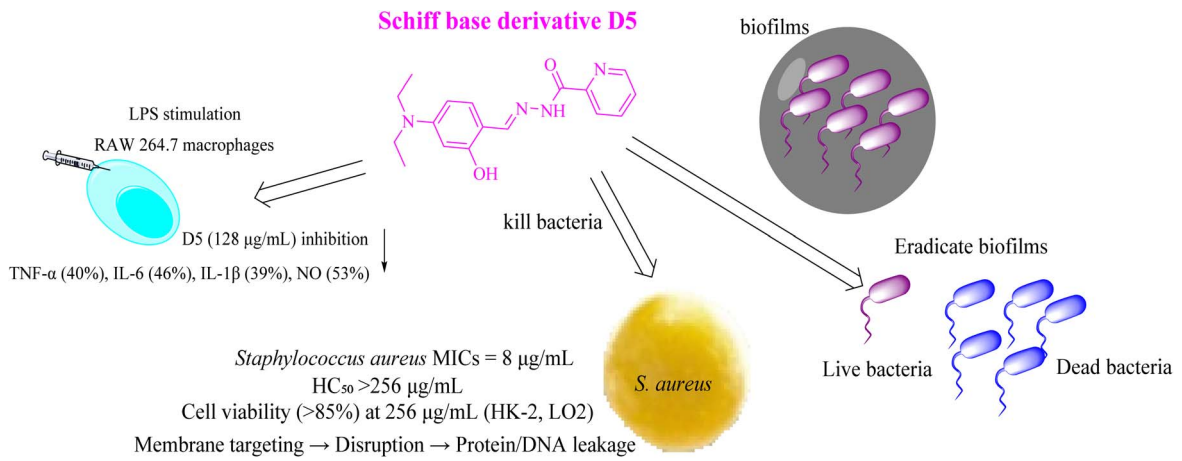

Fig. 1 Mechanism of action of compound **D5**.

by its electron-donating effect, and its potentially favorable physicochemical properties, we successfully constructed ten novel Schiff base derivatives through a classic, efficient condensation reaction with a series of structurally diverse amine derivatives (Fig. 1). The potential therapeutic value of these compounds in the specific clinical contexts of renal

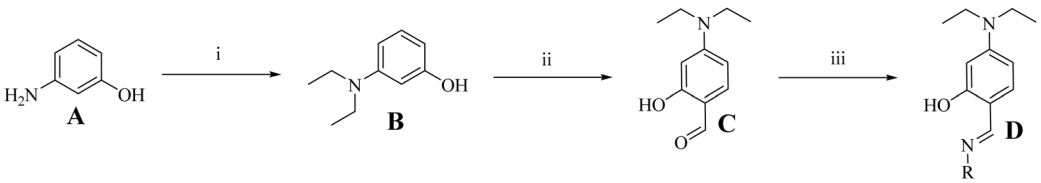

Scheme 1 Synthesis of Schiff base derivatives. Conditions and reagents: (i) ethanol, Na_2CO_3, bromoethane, rt; (ii) $POCl_3$, DMF, 75 °C, yield 70%; (iii) ethanol, different amine groups, reflux, yield 68–88%.

Table 1 Minimum inhibitory concentration (MIC)[a] [μg mL^{-1}] of triazole derivatives on reference bacterial strains

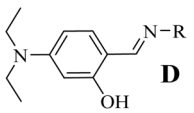

Compounds	R	*E. coli* ATCC 25922	*S. aureus* ATCC 29213	*S. aureus* ATCC 43300	*S. aureus* MRSA2
Vancomycin [b]	—	—	1	2	2
Enrofloxacin [c]	—	0.0625	—	—	—
C	—	>256	>256	>256	>256
D1	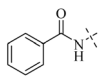	>256	>256	>256	>256
D2	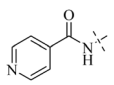	>256	>256	>256	>256
D3	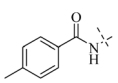	>256	>256	>256	>256
D4	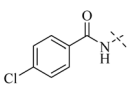	>256	>256	>256	>256
D5	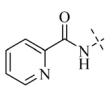	>256	8	8	8
D6	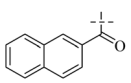	>256	128	128	128
D7	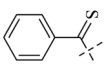	>256	128	128	128
D8	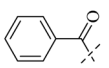	>256	128	128	128
D9	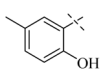	>256	>256	>256	>256
D10	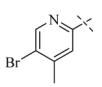	>256	>256	>256	>256

[a] The minimum inhibitory concentration (MIC) is the lowest concentration that completely inhibits microbial growth after 16–24 h. Each experiment was repeated three times. [b] **Vancomycin** is a clinical drug against Gram-positive bacteria. [c] **Enrofloxacin** is a broad-spectrum quinolone-based antibiotic.

abscess and lupus nephritis was then explored through *in vitro* activity evaluation.

2. Results and discussion

2.1 Chemical synthesis

This study successfully established an efficient, scalable three-step synthetic route for preparing a series of novel Schiff base derivatives (Scheme 1). The synthesis of the key intermediate, 3-hydroxy-*N*,*N*-diethylaniline, employed a selective *N*-alkylation strategy using bromoethane (in a sodium carbonate/anhydrous ethanol system), effectively avoiding competitive O-alkylation side reactions at the phenolic hydroxyl group. Subsequently, Vilsmeier–Haack formylation was conducted under precise temperature-controlled conditions to achieve *ortho*-formylation relative to the phenolic hydroxyl, yielding the key building block 4-(diethylamino)salicylaldehyde in 70% yield.[23,24] Finally, in a catalyst-free ethanol system, this aldehyde underwent condensation with 10 structurally diverse amines, affording the target Schiff base library in high yields (68–88%). All compounds were fully characterized by ^{1}H NMR, ^{13}C NMR, and mass spectrometry. This route features mild conditions, broad functional group compatibility, and avoids the need for column chromatography purification, establishing a robust chemical foundation for rapid structure–activity relationship studies of antibacterial and anti-inflammatory lead compounds.

Table 2 The activity of **D5** against clinically isolated bacterial strains

Compound	*B. subtilis* ATCC6633	*B. cereus* CMCC63303	*L. monocytogenes* CICC21662	*E. faecalis* ATCC29212	*S. aureus* LN38
Vancomycin	1	1	1	2	1
C	>256	>256	>256	>256	>256
D5	16	8	8	8	16

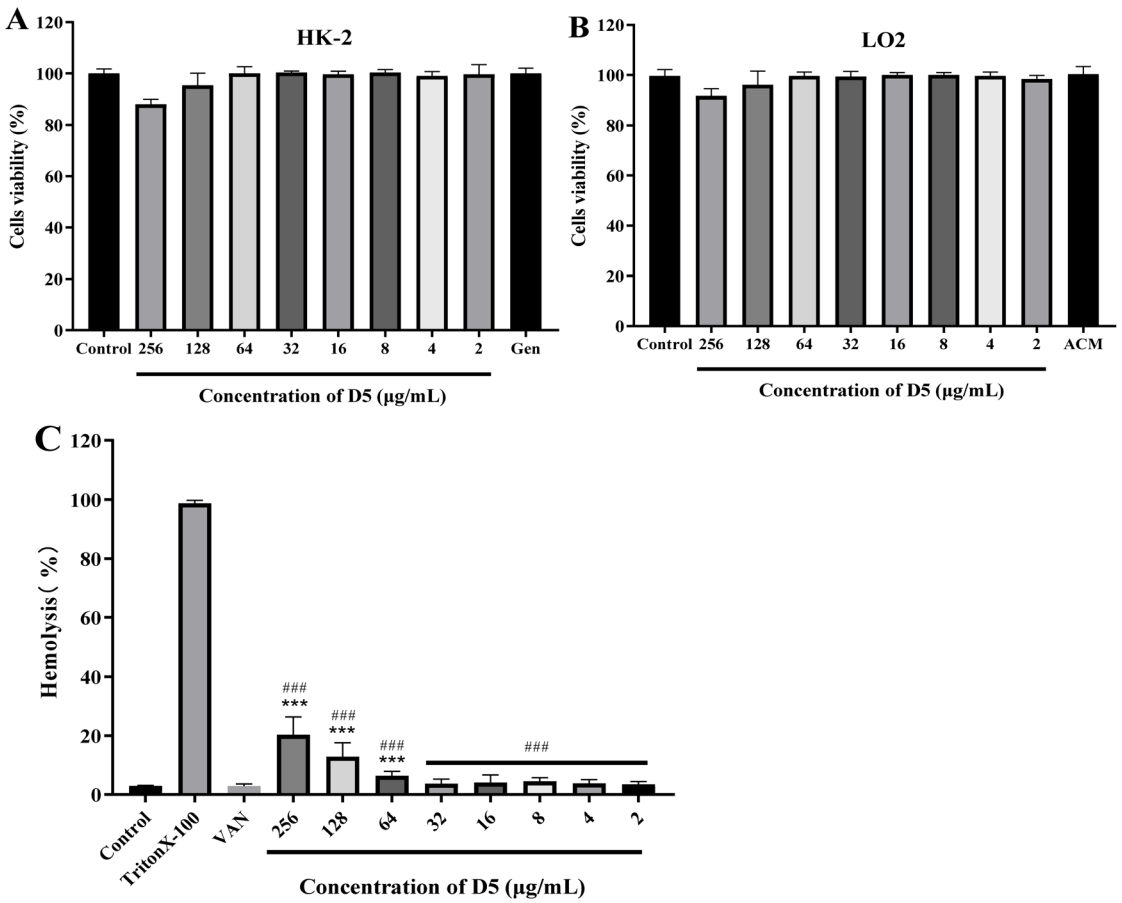

Fig. 2 (A) Cytotoxicity of compound **D5** against HK-2 cells after 24 h. (B) Cytotoxicity of compound **D5** against LO2 cells after 24 h. (C) Percentage of hemolysis of rabbit blood cells at various **Q10** concentrations. Difference is considered significant at $^{*}p < 0.05$, $^{**}p < 0.01$, $^{***}p < 0.001$. Compared with the control group; $^{\#}p < 0.05$, $^{\#\#}p < 0.01$, $^{\#\#\#}p < 0.001$ *vs.* model group. Data are presented as means ± SEM from three independent experiments. Gentamicin (Gen, 256 μg mL^{-1}), acetaminophen (ACM, 256 μg mL^{-1}) and **Vancomycin** (VAN, 256 μg mL^{-1}) were used as reference drugs.

2.2 The antibacterial activity of the compounds

We evaluated the *in vitro* antibacterial activity of the newly synthesized compounds using the minimum inhibitory concentration (MIC) method.[25] Target compound **D5** exhibited potent antibacterial activity against the standard strain of *S. aureus* ATCC 29213 and a clinically isolated methicillin-resistant *S. aureus* MRSA2 (Table 1). Its MIC value against MRSA2 was 8 μg mL^{-1}, significantly lower than that of the parent scaffold 4-(diethylamino)salicylaldehyde (MIC > 256 μg mL^{-1}), confirming **D5**'s *in vitro* antibacterial efficacy. However, activity against Gram-negative bacteria (*e.g.*, *Escherichia coli* ATCC 25922) was weak (MIC > 256 μg mL^{-1}). Subsequent testing of **D5** against other Gram-positive bacteria further demonstrated its excellent antibacterial activity, as shown in Table 2. Consequently, **D5** was selected for further investigation.

2.3 Cytotoxicity and hemolytic activity

Cytotoxicity toward mammalian cells and hemolytic activity are key indicators for assessing the safety profile of antimicrobial agents, evaluated *via* cell viability and HC_{50} (concentration inducing 50% hemolysis), respectively.[26] First, we determined that compound **D5** exhibits low toxicity against mammalian cell lines (human renal proximal tubular epithelial cells HK-2 and human normal hepatocytes LO2), maintaining >85% cell viability at 256 μg mL^{-1} (Fig. 2A and B). With a selectivity index (SI = IC_{50}/MIC) greater than 25, **D5** demonstrates a wide therapeutic window and favorable renal safety. Subsequently, the hemolytic activity of **D5** against rabbit red blood cells (RBCs) was assessed. Using 1% Triton X-100 as the positive control and sterile PBS as the negative control, compounds were incubated with 4% rabbit RBCs at 37 °C for 24 hours. As shown in Fig. 2C, **D5** at concentrations ranging from 2 to 256 μg mL^{-1} showed no hemolytic activity, demonstrating that it does not induce hemolysis in rabbit RBCs even at antibacterial concentrations.

2.4 Time-killing curve determinations

Building upon its potent bacteriostatic activity, **D5** demonstrated rapid and complete bactericidal effects against *S. aureus* ATCC 29213.[27] At a concentration of 8 × MIC (64 μg mL^{-1}), **D5** achieved >99.9% eradication of bacterial colonies within 10 hours (Fig. 3), indicating its capacity for swift microbial clearance. Crucially, in a continuous serial passage assay designed to evaluate resistance development potential, the MIC of **D5** against *S. aureus* ATCC 29213 increased only 16-fold after prolonged exposure. This modest increase stands in stark contrast to the rapid, significant MIC shifts typically observed with conventional antibiotics under selective pressure. Collectively, these results confirm that **D5** not only effectively kills *S. aureus* but also exhibits a low propensity for inducing resistance, a critical advantage for long-term therapeutic utility.

2.5 Inhibitory effects towards *S. aureus* biofilm formation

Recognizing that biofilm formation is a critical factor contributing to treatment failure in renal abscesses (by impeding antibiotic penetration and enabling immune evasion), we evaluated the impact of **D5** on *S. aureus* MRSA2 biofilms.[27] First, we assessed **D5**'s ability to inhibit biofilm formation using the crystal violet quantitative assay. As shown in Fig. 4A, **D5** demonstrated potent, concentration-dependent (2–256 μg mL^{-1}) inhibition of biofilm formation by *S. aureus* MRSA2, achieving >95% suppression at 64 μg mL^{-1} (8 × MIC). Crucially, we further investigated whether **D5** could eradicate pre-established mature biofilms. Following full biofilm development by MRSA2, treatment with **D5** for 24 hours (Fig. 4B) revealed significant biofilm eradication activity. **D5** achieved >95% clearance of mature biofilms at 128 μg mL^{-1} (16 × MIC), demonstrating its dual capability to not only prevent biofilm establishment but also effectively disrupt entrenched biofilm structures. This potent dual-action anti-biofilm profile positions **D5** as a promising candidate for overcoming biofilm-mediated persistence in complex infections like renal abscesses.

2.6 The anti-inflammatory activity of D5

To evaluate the potential of compound **D5** in mitigating renal inflammation – a critical pathological feature shared by pyelonephritis and lupus nephritis – we employed an LPS-stimulated

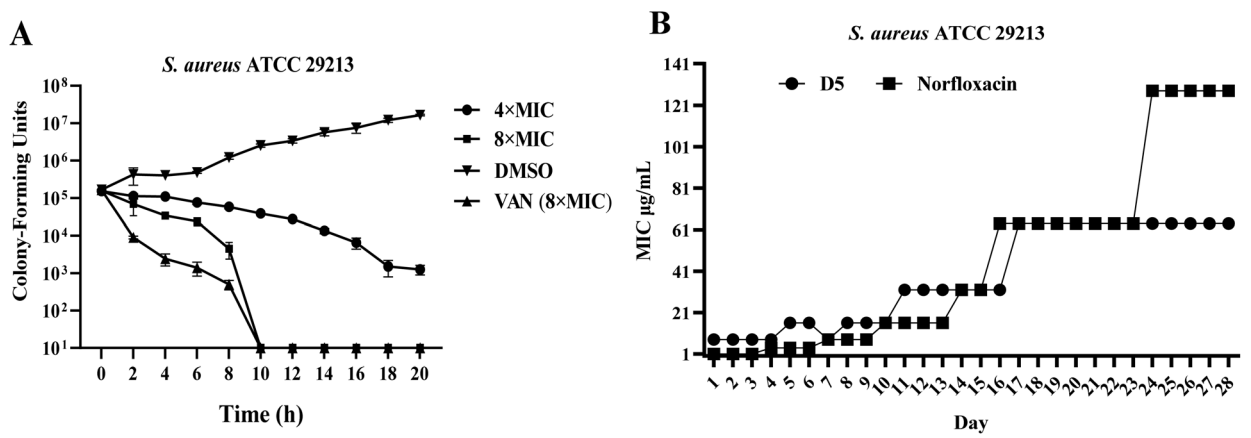

Fig. 3 (A) Time-kill kinetics of **D5** against *S. aureus* ATCC 29213. (B) Resistance development of **D5**. Data are presented as means ± SEM from three independent experiments. **Vancomycin** (VAN) and norfloxacin were used as reference drugs.

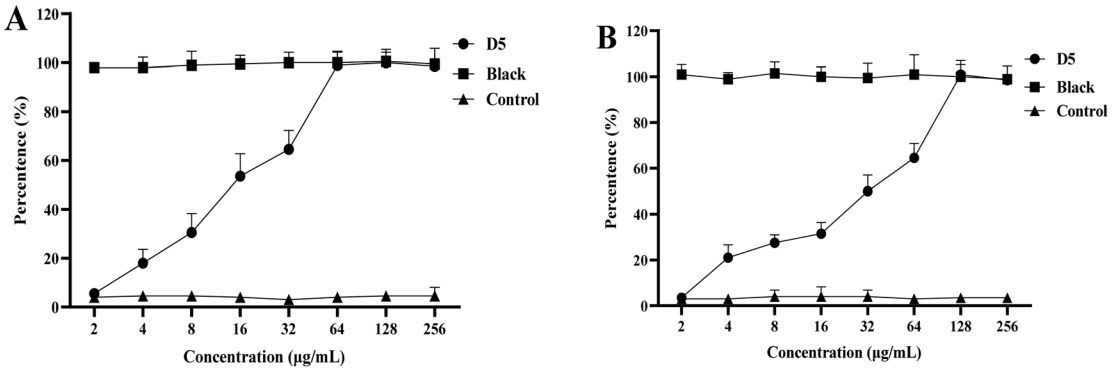

Fig. 4 Biofilm (A) inhibition and (B) eradication against *S. aureus* MRSA2 by compound **D5**. Data are presented as means ± SEM from three independent experiments.

RAW 264.7 macrophage model. This system effectively mimics pathogen-triggered inflammation in pyelonephritis and the dysregulated innate immune response characteristic of lupus nephritis. **D5** demonstrated potent, dose-dependent multi-target anti-inflammatory effects across key inflammatory pathways.[28] As illustrated in Fig. 5A, **D5** significantly suppressed TNF-α release (40% inhibition at 128 μg mL^{-1}), with activity emerging at concentrations as low as 8 μg mL^{-1}. Concurrently, it exhibited robust blockade of IL-6 secretion (46% inhibition at 128 μg mL^{-1}, Fig. 5B) and substantially inhibited NLRP3 inflammasome-mediated IL-1β production (39% inhibition at 128 μg mL^{-1}, Fig. 5C). Furthermore, **D5** effectively attenuated nitric oxide (NO) synthesis (53% reduction at 128 μg mL^{-1}, Fig. 5D), a key mediator of inflammatory tissue damage.

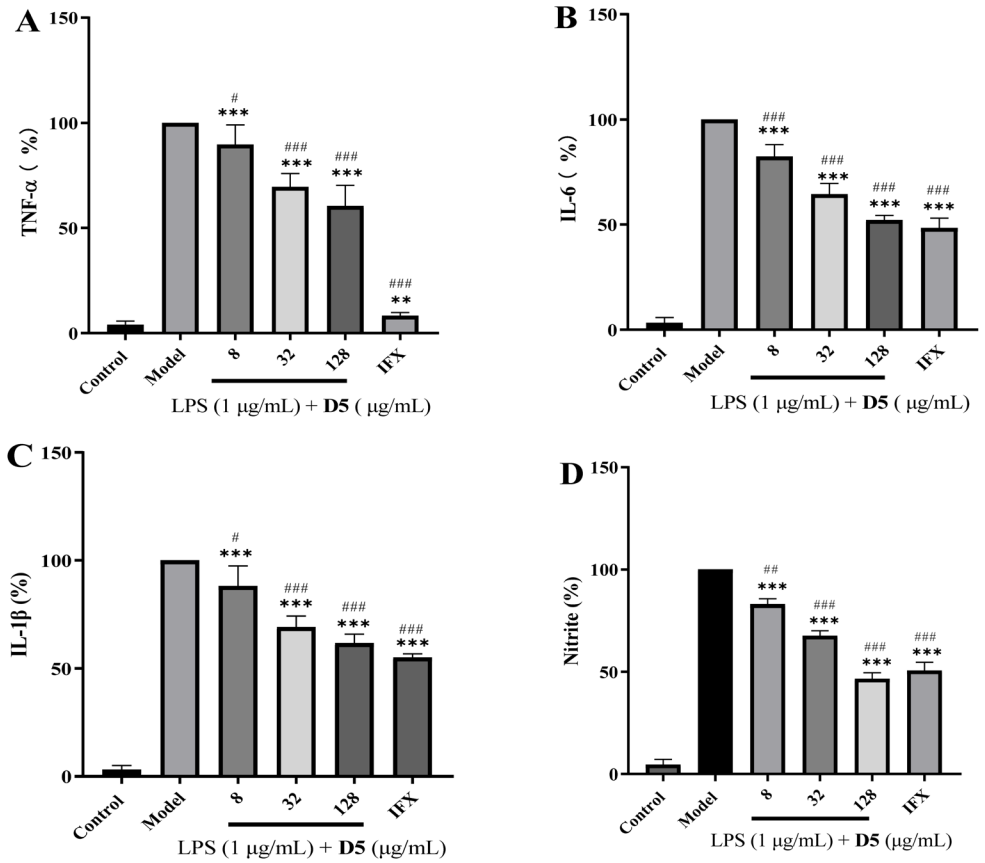

Fig. 5 Evaluation of anti-inflammatory properties in LPS-stimulated RAW 264.7 macrophages treated with compound **D5**. (A) Inhibition of pro-inflammatory cytokine TNF-α release by **D5**. (B) Attenuation of IL-6 accumulation by **D5**. (C) Inhibition of pro-inflammatory cytokine IL-1β production by **D5**. (D) Attenuation of nitrite accumulation by **D5**. Compared with the control group, $^{*}p < 0.05$, $^{**}p < 0.01$, $^{***}p < 0.001$; $^{\#}p < 0.05$, $^{\#\#}p < 0.01$, $^{\#\#\#}p < 0.001$ *vs.* LPS model group. Data are presented as means ± SEM from three independent experiments. Infliximab (IFX, 100 μg mL^{-1}) was used as a reference drug.

Notably, these anti-inflammatory effects occurred at concentrations well below cytotoxic levels (256 μg mL^{-1}), confirming **D5**'s capacity to simultaneously target multiple inflammatory cascades relevant to renal pathology without compromising cellular viability.

2.7 Antimicrobial mechanism investigation

To elucidate the membrane-targeting mechanism underpinning **D5**'s potent bactericidal activity, we employed a multimodal approach assessing bacterial membrane integrity and function. First, using a dual-dye strategy where DAPI stains all dsDNA (blue) and propidium iodide (PI) selectively labels compromised nuclei (red), we confirmed **D5** induces rapid membrane permeabilization in *S. aureus* ATCC 29213.[29,30] Treatment with **D5** at 4 × MIC (32 μg mL^{-1}) for just 2 hours resulted in near-complete PI uptake (Fig. 6A), starkly contrasting untreated controls. We further probed membrane functionality using $DiOC_2(3)$, a ratiometric fluorescent probe sensitive to membrane potential: depolarization reduces the red/green fluorescence ratio. **D5** treatment caused a significant decrease in this ratio (Fig. 6B), providing direct evidence of bacterial membrane depolarization. Crucially, to quantify the functional consequences of membrane disruption, we measured leakage of intracellular components. Following exposure to increasing concentrations of **D5**, *S. aureus* ATCC 29213 exhibited dose-dependent efflux of proteins and DNA into the culture medium (Fig. 6C and D). This correlated release of vital macromolecules – reaching levels significantly higher than untreated controls – mechanistically explains **D5**'s rapid bactericidal action, as sustained membrane compromise leads to catastrophic loss of cellular homeostasis.

2.8 The drug-likeness evaluation of D5

Drug-likeness assessment – a pivotal early-stage filter in pharmaceutical discovery that prioritizes lead compounds through evaluation of key physicochemical and pharmacokinetic properties – was conducted for **D5** (Table 3). Plasma protein binding (PPB) analysis revealed high affinity binding (86.6% at the therapeutically relevant concentration of 30 μM). While this

Table 3 Partial drug likeness data for **D5**

Compound	PPB	$\log D_{7.4}$
D5	86.6%	3.48 ± 0.13

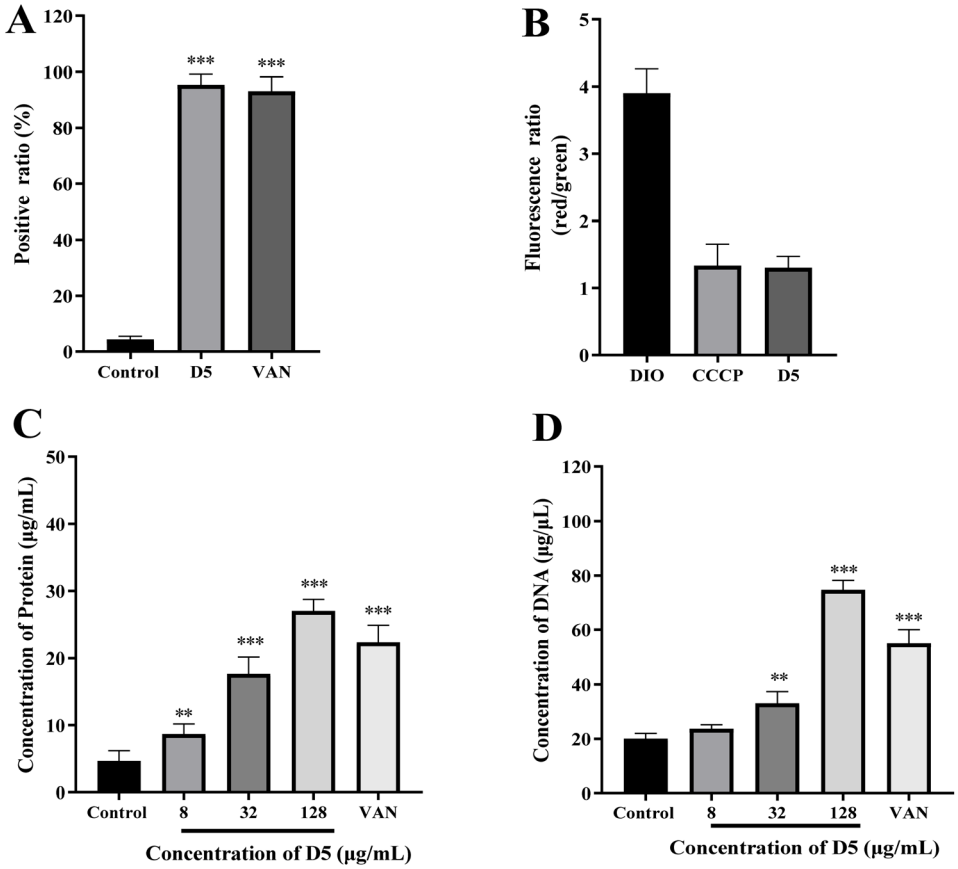

Fig. 6 (A) **D5**-induced membrane permeability changes in *S. aureus* ATCC 29213. (B) **D5**-induced membrane depolarization in *S. aureus* ATCC 29213. (C) Protein leakage caused by the treatment of **D5** on *S. aureus* ATCC 29213. (D) DNA leakage resulting from the treatment of **D5** on *S. aureus* ATCC 29213. $^{*}p < 0.05$, $^{**}p < 0.01$, $^{***}p < 0.001$. Data are presented as means ± SEM from three independent experiments. CCCP (depolarization control). **Vancomycin** (VAN, 2 μg mL^{-1}) was used as a reference drug.

may reduce free drug concentration, it could potentially prolong antimicrobial exposure through depot effects in circulation. Lipophilicity, quantified as $\log D_{7.4} = 3.48 \pm 0.13$, complies with Lipinski's rule of five criteria and indicates favorable membrane permeability – a critical attribute for penetrating renal parenchymal sites and bacterial biofilms. Significantly, this $\log D$ range aligns with optimal pharmacokinetic profiles for renal-targeted therapeutics. Building upon **D5**'s established safety profile, dual-target antibacterial/anti-inflammatory efficacy, and compliant drug-like properties, it emerges as a high-priority candidate compound. Subsequent medicinal chemistry optimization should focus on pharmacokinetic refinement (particularly modulating PPB) while preserving its unique multi-mechanistic pharmacology for advanced development toward complex renal infections.

3. Conclusions

This study successfully constructed a library of Schiff base derivatives based on the 4-(diethylamino)salicylaldehyde scaffold, with compound **D5** emerging as a multi-faceted therapeutic candidate. **D5** exhibits potent antibacterial activity against *S. aureus* (ATCC 29213; MIC = 8 μg mL^{-1}), exerting its effects through bacterial membrane depolarization and permeabilization, which triggers leakage of intracellular proteins and DNA. It achieves complete bactericidal eradication within 10 hours at 8 × MIC concentration while demonstrating low resistance induction potential. Crucially, **D5** effectively inhibits biofilm formation and eradicates pre-established *S. aureus* biofilms, disrupting this key resistance mechanism. Furthermore, in LPS-stimulated RAW 264.7 macrophages – modeling renal infection-related inflammation – **D5** significantly downregulates key pro-inflammatory mediators (TNF-α, IL-6, IL-1β, and NO), revealing its immunomodulatory effects relevant to nephritis. Notably, **D5** displays exceptional selectivity, showing low cytotoxicity toward mammalian cells (HK-2/LO2) and no significant hemolysis at 256 μg mL^{-1}, yielding a favorable selectivity index. Its physicochemical properties comply with Lipinski's rule of five, establishing a foundation for druggability. Collectively, **D5** represents a multi-target candidate uniquely integrating direct antibacterial action with immunomodulatory capacity. This dual functionality confers substantial translational potential for treating nephritis complicated by bacterial infections. Future work will focus on pharmacokinetic refinement and *in vivo* efficacy validation to advance this promising compound.

4. Experimental section

4.1 Chemically synthetical experiments

All final products were characterized by ^{1}H NMR (400 MHz) and ^{13}C NMR (100 MHz) spectroscopy using a Bruker avance 400 spectrometer. Chemical shifts are reported in parts per million (ppm) referenced to residual solvent peaks as internal standards (DMSO-d_6: δ 2.50 for ^{1}H NMR, δ 40.0 for ^{13}C NMR).

4.1.1 3-(diethylamino)phenol (B). A mixture of 3-aminophenol (2.14 g, 19.6 mmol), ethyl bromide (6 g, 55 mmol), and sodium carbonate dissolved in anhydrous ethanol (10 mL) was stirred at room temperature for 72 hours. The resulting solution was then filtered, and the filtrate was concentrated under vacuum to afford the crude product, which was used in the subsequent reaction without further purification.[23,24]

4.1.2 4-(diethylamino)-2-hydroxybenzaldehyde (C). A solution of phosphorus oxychloride ($POCl_3$) (2.75 mL, 0.03 mol) was slowly added to *N*,*N*-dimethylformamide (DMF) (3.65 mL, 0.05 mol) at 5–10 °C with continuous stirring. To this cooled reagent mixture, a solution of 3-(*N*,*N*-diethylamino)phenol (0.01 mol) in DMF (6 mL) was slowly added with constant stirring. The resulting mixture was heated at 75 °C for 4 hours. After cooling to room temperature, the reaction mixture was poured into ice-cold water (60 mL), neutralized with aqueous sodium carbonate solution, and extracted to yield a brown solid.[23,24] The crude product was filtered, washed with cold water, dried, and recrystallized from ethanol to afford pure product C in 70% yield.

4.1.3 *N*′-(4-(diethylamino)-2-hydroxybenzylidene) benzohydrazide (D1). Compound **C** (1 mmol) was dissolved in anhydrous ethanol, followed by the addition of benzoyl hydrazine (1 mmol). The mixture was refluxed overnight. Upon reaction completion, the solvent was evaporated under reduced pressure. The crude product was recrystallized from ethanol to afford the final product **D1**. Compounds **D2–D12** were prepared using an analogous procedure by reacting compound **C** with their respective amine derivatives.

Yield, 75%. White solid. ^{1}H NMR (400 MHz, DMSO-d_6) δ 11.79 (s, ^{1}H), 11.48 (s, ^{1}H), 8.43 (s, ^{1}H), 7.91 (d, J = 7.6 Hz, 2H), 7.59–7.52 (m, 3H), 7.19 (d, J = 8.7 Hz, ^{1}H), 6.27 (d, J = 7.4 Hz, ^{1}H), 6.13 (s, ^{1}H), 3.38–3.33 (m, 4H), 1.10 (t, J = 6.9 Hz, 6H). ^{13}C NMR (101 MHz, DMSO-d_6) δ 162.17, 159.70, 150.14, 150.00, 131.59, 128.43, 127.42, 106.42, 103.62, 97.51, 43.75, 12.50. TOF-MS, *m*/*z*: $[M + H]^+$, calcd. for $C_{18}H_{22}N_3O_2^+$, 312.1712, found: 312.1715.

4.1.4 *N*′-(4-(diethylamino)-2-hydroxybenzylidene) isonicotinohydrazide (D2). Yield, 78%. White solid. ^{1}H NMR (400 MHz, DMSO-d_6) δ 12.00 (s, ^{1}H), 11.28 (s, ^{1}H), 8.78 (s, 2H), 8.45 (s, ^{1}H), 7.82 (d, J = 5.7 Hz, 2H), 7.24 (d, J = 8.8 Hz, ^{1}H), 6.28 (dd, J = 8.8, 2.2 Hz, ^{1}H), 6.14 (d, J = 2.1 Hz, ^{1}H), 3.36 (dd, J = 14.1, 7.0 Hz, 4H), 1.11 (t, J = 7.0 Hz, 6H). ^{13}C NMR (101 MHz, DMSO-d6) δ 160.56, 159.75, 150.83, 150.27, 140.24, 131.58, 121.36, 106.26, 103.77, 97.42, 43.78, 12.50. TOF-MS, *m*/*z*: $[M + H]^+$, calcd. for $C_{17}H_{21}N_4O_2^+$, 313.1664, found: 313.1668.

4.1.5 *N*′-(4-(diethylamino)-2-hydroxybenzylidene)-4-methylbenzohydrazide (D3). Yield, 88%. White solid. ^{1}H NMR (400 MHz, DMSO-d_6) δ 11.72 (s, ^{1}H), 11.51 (s, ^{1}H), 8.42 (s, ^{1}H), 7.83 (d, J = 7.8 Hz, 2H), 7.33 (d, J = 7.8 Hz, 2H), 7.18 (d, J = 8.7 Hz, ^{1}H), 6.26 (d, J = 8.2 Hz, ^{1}H), 6.13 (s, ^{1}H), 3.35 (d, J = 6.1 Hz, 4H), 2.37 (s, 3H), 1.10 (t, J = 6.9 Hz, 6H). ^{13}C NMR (101 MHz, DMSO-d_6) δ 161.82, 159.48, 149.88, 149.58, 141.42, 131.36, 130.05, 128.75, 127.23, 103.38, 97.32, 43.54, 20.76, 12.29. TOF-MS, *m*/*z*: $[M + H]^+$, calcd. for $C_{19}H_{24}N_3O_2^+$, 326.1868, found: 326.1871.

4.1.6 4-Chloro-*N*′-(4-(diethylamino)-2-hydroxybenzylidene) benzohydrazide (D4). Yield, 70%. White solid. ^{1}H NMR (400 MHz, DMSO-d_6) δ 11.85 (s, ^{1}H), 11.40 (s, ^{1}H), 8.42 (s, ^{1}H), 7.93 (d,

J = 8.4 Hz, 2H), 7.60 (d, J = 8.4 Hz, 2H), 7.20 (d, J = 8.7 Hz, ^{1}H), 6.27 (d, J = 10.7 Hz, ^{1}H), 6.12 (s, ^{1}H), 3.41–3.33 (m, 4H), 1.10 (t, J = 6.9 Hz, 6H). ^{13}C NMR (101 MHz, DMSO-d_6) δ 161.09, 159.71, 150.20, 136.42, 131.88, 131.58, 129.35, 128.53, 106.37, 103.66, 97.48, 43.76, 12.50. TOF-MS, m/z: $[M + H]^+$, calcd. for $C_{18}H_{21}ClN_3O_2^+$, 346.1322, found: 346.1327.

4.1.7 *N*′-(4-(diethylamino)-2-hydroxybenzylidene) picolinohydrazide (D5). Yield, 72%. White solid. ^{1}H NMR (400 MHz, DMSO-d_6) δ 12.16 (s, ^{1}H), 11.57 (s, ^{1}H), 8.82–8.55 (m, 2H), 8.08 (dd, J = 20.1, 7.2 Hz, 2H), 7.79–7.50 (m, ^{1}H), 7.12 (d, J = 8.7 Hz, ^{1}H), 6.27 (d, J = 8.7 Hz, ^{1}H), 6.12 (s, ^{1}H), 3.40–3.33 (m, 4H), 1.11 (t, J = 6.9 Hz, 6H). ^{13}C NMR (101 MHz, DMSO-d_6) δ 159.84, 159.61, 151.42, 150.21, 149.47, 148.45, 137.92, 131.84, 126.80, 122.49, 106.44, 103.65, 97.51, 43.76, 12.50. TOF-MS, m/z: $[M + H]^+$, calcd. for $C_{18}H_{21}ClN_3O_2^+$, 313.1664, found: 313.1666.

4.1.8 *N*-(4-(diethylamino)-2-hydroxybenzylidene)-2-naphthamide (D6). Yield, 79%. White solid. ^{1}H NMR (400 MHz, DMSO-d_6) δ 11.96 (s, ^{1}H), 11.50 (s, ^{1}H), 8.50 (d, J = 19.5 Hz, 2H), 8.03 (dt, J = 26.3, 7.4 Hz, 4H), 7.76–7.55 (m, 2H), 7.22 (d, J = 8.7 Hz, ^{1}H), 6.28 (d, J = 8.6 Hz, ^{1}H), 6.15 (s, ^{1}H), 3.42–3.34 (m, 4H), 1.11 (t, J = 6.9 Hz, 6H). ^{13}C NMR (101 MHz, DMSO-d_6) δ 169.34, 165.04, 159.50, 158.29, 155.84, 150.05, 148.85, 143.90, 131.43, 129.15, 107.12, 106.30, 103.94, 103.56, 97.47, 78.08, 43.75, 42.29, 41.24, 28.17, 12.49. TOF-MS, m/z: $[M + H]^+$, calcd. for $C_{22}H_{23}N_2O_2^+$, 347.1759, found: 347.1762.

4.1.9 *N*-(4-(diethylamino)-2-hydroxybenzylidene) benzothioamide (D7). Yield, 70%. White solid. ^{1}H NMR (400 MHz, DMSO-d_6) δ 11.26 (s, ^{1}H), 10.19 (s, 2H), 9.78 (s, 2H), 9.61 (s, ^{1}H), 8.65 (d, J = 5.0 Hz, 5H), 7.70 (d, J = 5.0 Hz, 5H), 7.42 (d, J = 8.9 Hz, ^{1}H), 6.35 (s, ^{1}H), 6.04 (s, ^{1}H), 3.45–3.37 (m, 4H), 1.11 (t, J = 7.0 Hz, 6H). ^{13}C NMR (101 MHz, DMSO-d_6) δ 198.51, 190.88, 150.23, 146.47, 134.23, 121.00 , 104.68, 96.14, 44.32, 12.62. TOF-MS, m/z: $[M + H]^+$, calcd. for $C_{18}H_{21}N_2OS^+$, 313.1374, found: 313.1378.

4.1.10 *N*-(4-(diethylamino)-2-hydroxybenzylidene) benzamide (D8). Yield, 81%. White solid. ^{1}H NMR (400 MHz, DMSO-d_6) δ 11.28 (s, ^{1}H), 9.60 (s, ^{1}H), 7.41 (d, J = 8.9 Hz, ^{1}H), 6.33 (d, J = 8.9 Hz, ^{1}H), 6.14–5.97 (m, ^{1}H), 3.39 (q, J = 7.0 Hz, 5H), 1.10 (t, J = 7.0 Hz, 6H). ^{13}C NMR (101 MHz, DMSO-d_6) δ 190.68, 163.40, 153.78, 134.02, 111.20, 104.43, 95.92, 44.09, 12.36. TOF-MS, m/z: $[M + H]^+$, calcd. for $C_{18}H_{21}N_2O^+$, 297.1603, found: 297.1607.

4.1.11 2-((4-(diethylamino)-2-hydroxybenzylidene)amino)-4-methylphenol (D9). Yield, 79%. White solid. ^{1}H NMR (400 MHz, DMSO-d_6) δ 8.62 (s, ^{1}H), 7.24 (d, J = 8.8 Hz, ^{1}H), 7.10 (s, ^{1}H), 6.81 (s, 2H), 6.25 (d, J = 8.0 Hz, ^{1}H), 5.96 (s, ^{1}H), 3.46–3.31 (m, 4H), 2.23 (s, 3H), 1.11 (t, J = 6.9 Hz, 6H). ^{13}C NMR (101 MHz, DMSO-d_6) δ 165.93, 158.25, 151.61, 147.70, 134.08, 133.87, 128.20, 126.50, 118.85, 116.01, 109.06, 103.64, 97.26, 43.84, 20.21, 12.58. TOF-MS, m/z: $[M + H]^+$, calcd. for $C_{18}H_{23}N_2O_2^+$, 299.1759, found: 299.1764.

4.1.12 2-(((5-bromo-4-methylpyridin-2-yl)imino)methyl)-5-(diethylamino)phenol (D10). Yield, 68%. White solid. ^{1}H NMR (400 MHz, DMSO-d_6) δ 9.19 (s, ^{1}H), 8.49 (s, ^{1}H), 7.91 (s, 2H), 7.41 (d, J = 8.9 Hz, ^{1}H), 7.31 (s, ^{1}H), 3.41 (q, J = 6.8 Hz, 4H), 2.37 (s, 3H), 1.13 (t, J = 6.8 Hz, 6H). ^{13}C NMR (101 MHz, DMSO-d_6) δ 161.81, 149.29, 148.14, 135.06, 120.40, 109.55, 104.37, 96.47, 43.78, 21.44, 12.32. TOF-MS, m/z: $[M + H]^+$, calcd. for $C_{17}H_{21}BrN_3O^+$, 362.0868, found: 362.0871.

4.2 Determination of minimum inhibitory concentration

The minimum inhibitory concentrations (MICs) of all test compounds were determined using the broth microdilution method following Clinical and Laboratory Standards Institute (CLSI) guidelines.[25] Bacterial strains were cultured in Mueller–Hinton broth (MHB) on a shaker at 37 °C for approximately 5 hours, then diluted to ~10^5 CFU mL^{-1} in a 96-well microtiter plate. Test compounds were serially diluted (0.05–256 μg mL^{-1}) in the plate, which was incubated at 37 °C for 18 h. The MIC was defined as the lowest concentration showing no visible growth. All tests were performed in triplicate.

4.3 Time-killing kinetics

Time-kill curve analysis of compound **D5** against *S. aureus* ATCC 29213 was performed according to CLSI guidelines.[27] Briefly, mid-log phase cultures grown in Mueller–Hinton broth (MHB) at 37 °C with shaking (200 rpm) were adjusted to 1 × 10^6 CFU mL^{-1} in pre-warmed MHB. Following vortex mixing, samples were incubated at 37 °C with shaking. Aliquots (100 μL) were collected at 0, 2, 4, 6, 8, 12, and 24 h, serially diluted in sterile PBS (pH 7.4), and plated (50 μL) on Mueller–Hinton agar. After 18–24 h incubation at 37 °C, viable colonies were enumerated (limit of detection: 100 CFU mL^{-1}). Experiments were performed in biological triplicate with starting inocula verified by spiral plating; compound sterility was confirmed in parallel incubations.

4.4 Drug resistance study

The resistance development study of compound **D5** was conducted following our established protocol.[27] According to the aforementioned methodology, the initial MIC of **D5** against *S. aureus* ATCC 29213 was determined. This sub-MIC passage procedure was consecutively repeated for 28 days.

4.5 Hemolysis assay

The hemolysis assay was adapted from a reported method.[26] Briefly, 100 μL of **D5** (serial concentrations in PBS) was combined with 100 μL of 4% defibrinated rabbit erythrocytes in PBS, yielding final concentrations of 2–256 μg mL^{-1}. Controls included 1% Triton X-100 (positive) and sterile PBS (negative). After 1 h incubation at 37 °C, erythrocytes were pelleted by centrifugation (1000×g, 5 min), and supernatant absorbance was measured at 490 nm. Hemolysis percentage was calculated as: hemolysis (%) = (sample − PBS)/(Triton − PBS) × 100% × 100%. Experiments were performed in triplicate.

4.6 Cytotoxicity assay

Cytotoxicity assessment was performed using the Cell Counting Kit-8 (CCK-8) according to established protocols with minor modifications.[26] Briefly, cells were seeded in 96-well plates and allowed to adhere overnight. Test compound **D5** was then added at designated concentrations and incubated for at 37 °C under

5% CO_2. Following treatment, 10 μL of CCK-8 reagent was added to each well, and plates were incubated for at 37 °C. Absorbance was measured at 450 nm using a microplate reader, with wells containing culture medium and CCK-8 reagent serving as the blank control. Cell viability was calculated using the formula: cell viability (%) = (OD_{450} sample value − OD_{450} blank hole value)/(OD_{450} value of untreated control − OD_{450} blank hole value) × 100%.

4.7 Biofilm formation assay

Biofilm biomass was quantified by crystal violet staining.[27] *S. aureus* MRSA2 was diluted 1 : 100 in fresh TSB with 1% (w/v) glucose, then co-incubated with compound **D5** (256–2 μg mL^{-1}) in glucose-supplemented TSB (200 μL per well) for 24 h at 37 °C. Control wells received equivalent DMSO. After removal of planktonic cells, adherent biofilms were gently rinsed (3 × PBS), air-dried, stained with 0.1% crystal violet (15 min), and rinsed again. Bound dye was solubilized in 95% ethanol (200 μL), and absorbance measured at 595 nm. Biofilm inhibition was calculated as: biofilm inhibition (%) = ($OD_{control}$ − OD_{sample})/$OD_{control}$ × 100. All experiments included triplicate replicates.

Biofilm eradication assays were adapted from established protocols with modifications.[27] Mature *S. aureus* MRSA2 biofilms were formed in 96-well plates (37 °C, 12 h). After removing planktonic cells, biofilms were treated with test compounds for 12 h at 37 °C. Biomass quantification followed the crystal violet staining/destaining protocol described for biofilm inhibition assays. The minimal biofilm eradication concentration (MBEC) was defined as the lowest compound concentration achieving ≥90% biomass reduction compared to untreated controls. Eradication efficiency was calculated as: % reduction = ($OD_{control}$ − OD_{sample})/$OD_{control}$ × 100. Triplicate measurements were performed throughout. All experiments were performed in triplicate.

4.8 The anti-inflammatory activity of D5

The anti-inflammatory activity of compound **D5** was evaluated in lipopolysaccharide (LPS)-stimulated RAW 264.7 macrophages.[28] Cells were seeded in 96-well plates (5 × 10^4 cells per well) and allowed to adhere overnight in complete DMEM (10% FBS). After pretreatment with **D5** at designated concentrations (*e.g.*, 1–64 μg mL^{-1}) for 2 h, inflammation was induced by adding LPS (*e.g.*, 100 ng mL^{-1}) and incubating for 24 h at 37 °C under 5% CO_2. Cell culture supernatants were then collected and analyzed for inflammatory mediators: TNF-α, IL-6, and IL-1β levels were quantified using commercial ELISA kits according to manufacturer protocols. Nitric oxide (NO) production using a commercial detection kit per manufacturer's protocol. All treatments included vehicle controls (*e.g.*, 0.1% DMSO) and were performed with ≥3 biological replicates.

4.9 Membrane potential and permeability assay

S. aureus ATCC 29213 was cultured overnight, diluted to logarithmic phase (OD_{600} = 0.4), harvested by centrifugation, and resuspended in PBS.[29] Bacterial suspensions were adjusted to 10^6–10^7 CFU mL^{-1}. Membrane potential was assessed using the BacLight™ Bacterial Membrane Potential Kit. Suspensions were incubated with 10 μM CCCP (depolarization control) or test compounds for 15 min (RT, dark). $DIOC_2(3)$ (10 μL) was then added, followed by 30 min incubation (RT, dark). Membrane permeability was evaluated using TO-PRO-3 iodide. Bacterial suspensions were stained with TO-PRO-3 (final concentration 1 μM), incubated 15 min (RT, dark), and analyzed by flow cytometry (30 000 events/sample). All experiments were performed in triplicate.

4.10 DNA and protein leakage

The assessment of cellular component leakage was adapted from established methodologies.[30]

S. aureus ATCC 29213 suspensions (2 × 10^6 CFU mL^{-1} in appropriate growth medium) were treated with **D5** at final concentrations corresponding to 16 ×, 4 ×, 1 × MIC. Following 4 h incubation at 37 °C with agitation, bacterial cells were pelleted by centrifugation (12 000×*g*, 10 min, 4 °C). The supernatant was carefully collected and filtered through 0.22-μm membranes to remove residual cells. Extracellular DNA concentration was quantified by measuring absorbance at 260 nm using a microvolume spectrophotometer. Concurrently, supernatant protein content was determined using a BCA Protein Assay Kit according to the manufacturer's protocol, with absorbance measured at 562 nm. All treatments included vehicle controls and were performed in technical triplicates.

4.11 Drug developability studies

The plasma protein binding rate of **D5** was determined *via* equilibrium dialysis.[31] Pre-hydrated dialysis bags were prepared by sealing one end. Each bag received 0.5 mL of blank Sprague–Dawley rat plasma and was securely sealed. Bags were suspended in centrifuge tubes containing 40 mL of PBS dialysate spiked with **D5** (30 μM). Following incubation at 37 °C with constant shaking (100 rpm) for 24 h to achieve equilibrium, samples from both compartments were collected. **D5** concentrations were quantified by HPLC. Binding percentage was calculated as: plasma protein binding rate (%) = [(*A* − *B*)/*A*] × 100%, where *A* is the total drug concentration inside the dialysis bag and *B* is the free drug concentration in the dialysate. All experiments included nonspecific binding controls and were performed in triplicate.

Log $D_{7.4}$ of compound **D5** was determined *via* the shake-flask method.[32] Briefly, 1 mg of **D5** was dissolved in 2 mL pH 7.4 buffer-saturated *n*-octanol, mixed with 2 mL *n*-octanol-saturated buffer, vortexed vigorously (3 min), and equilibrated (200 rpm, 24 h, 37 °C). After centrifugation and phase separation, aliquots from both phases were diluted in methanol (octanol phase: *x*; aqueous phase: *y*) and analyzed by HPLC. Log $D_{7.4}$ was calculated as: [log(the peak area of compound)$_{octanol}$ × *x*/(the peak area of compound)$_{buffer}$ × *y*]. All measurements were performed in triplicate.

4.12 Statistical analysis

Data represent mean ± SEM from at least three independent experiments. Statistical analyses were performed using SPSS

21.0 software. Differences between treatment groups were assessed by one-way ANOVA followed by post-hoc Tukey's test, with $p < 0.05$ considered statistically significant.

Conflicts of interest

The authors declare that the research was conducted in the absence of any commercial or financial relationships that could be construed as a potential conflict of interest.

Data availability

Data will be made available on request.

Supplementary information is available: ^{1}H and ^{13}C NMR spectra of all final products. See DOI: **https://doi.org/10.1039/d5ra05377c**.

References

1 P. L. Conan, I. Podglajen, F. Compain, M. Osman, D. Lebeaux and E. Flamarion, *Infect. Dis.*, 2021, **53**(2), 131–136.
2 Z. Zhan, X. Lin, G. Li, J. Zeng, D. Su, J. Liao and Q. Shen, *Medicine*, 2023, **102**(48), e36355.
3 C. Yu, P. Li, X. Dang, X. Zhang, Y. Mao and X. Chen, *J. Autoimmun.*, 2022, **132**, 102871.
4 N. Alforaih, L. Whittall-Garcia, Z. Touma and J. Appl, *Lab. Med.*, 2022, **7**(6), 1450–1467.
5 P. Pietrucha-Dilanchian and T. M. Hooton, *Microbiol. Spectrum*, 2016, **4**(6), 41–68.
6 N. Ahmad-Mansour, P. Loubet, C. Pouget, C. Dunyach-Remy, A. Sotto and J. P. Lavigne, *Toxins*, 2021, **13**(10), 677.
7 L. Tian, T. Qiang, J. Xia, B. Zhang, Q. Lu, Y. Liu, J. Hu, K. Kang, J. Li, J. Zhang, X. Yang, Y. Wang, D. Zhang, H. Gao and C. Liang, *J. Med. Chem.*, 2025, **68**(3), 3335–3355.
8 E. Christaki, M. Marcou and A. Tofarides, *J. Mol. Evol.*, 2020, **88**(1), 26–40.
9 K. B. Ita, *Curr. Drug Delivery*, 2015, **12**(6), 645–651.
10 J. Yan and B. L. Bassler, *Cell Host Microbe*, 2019, **26**(1), 15–21.
11 Z. Wu, T. Zhang, X. Ma, S. Guo, Q. Zhou, A. Zahoor and G. Deng, *Inflammopharmacology*, 2023, **31**(6), 2901–2937.
12 Q. Ren, F. Guo, S. Tao, R. Huang, L. Ma and P. Fu, *Biomed. Pharmacother.*, 2020, **122**, 109772.
13 M. Kaur, S. Kumar, M. Yusuf, J. Lee, A. K. Malik, Y. Ahmadi and K. H. Kim, *Environ. Res.*, 2023, **236**(Pt 2), 116811.
14 B. Musikavanhu, Y. Liang, Z. Xue, L. Feng and L. Zhao, *Molecules*, 2023, **28**(19), 6960.
15 M. Coandă, C. Limban and D. C. Nută, *Antibiotics*, 2024, **13**(1), 75.
16 M. Barua, S. Bandyopadhyay, A. Wasai, M. Ghosh, I. Roy, P. Ghosh, S. Koner, C. Rizzoli, A. Roy, S. Saha and S. Mandal, *Microb. Pathog.*, 2024, **188**, 106548.
17 G. L. Backes, B. S. Jursic and D. M. Neumann, *Bioorg. Med. Chem.*, 2015, **23**(13), 3397–3407.
18 M. Kumar, A. K. Singh and V. K. Singh, *Coord. Chem. Rev.*, 2024, **505**, 59.
19 J. Camacho, C. A. Bejarano, J. E. Diaz, Y. Vargas-Casanova, S. K. Carvajal, V. Diaz Santoyo, C. M. Parra-Giraldo and A. E. Loaiza, *Molecules*, 2025, **30**(5), 1165.
20 S. Hashmi, S. Khan, Z. Shafiq, P. Taslimi, M. Ishaq, N. Sadeghian, H. S. Karaman, N. Akhtar, M. Islam, A. Asari, H. Mohamad and İ. Gulçin, *Bioorg. Chem.*, 2021, **107**, 104554.
21 T. Itomirov, F. Dimiza, I. Z. Matić, T. Stanojković, A. Pirković, L. Živković, B. Spremo-Potparević, I. Novaković, K. Anđelković, M. Milčić, G. Psomas and M. Š. Ristović, *J. Inorg. Biochem.*, 2022, **235**, 111942.
22 S. Huang, X. Yang, J. Zhao, M. Zeeshan, C. Wang, D. Yang, X. Han and G. Zhang, *Pestic. Biochem. Physiol.*, 2025, **212**, 106444.
23 C. C. Jiménez, N. Farfán, M. Romero-Avila, M. Rodríguez, L. Aparicio-Ixta, G. Ramos-Ortiz and M. E. Ochoa, *J. Organomet. Chem.*, 2014, **755**, 33–40.
24 S. B. Chemate and N. Sekar, *J. Fluoresc.*, 2015, **25**(6), 1615–1628.
25 Y. Zhong, F. Chen, D. Chen, Q. He, X. Zhang, L. Lan and C. Yang, *NPJ Antimicrob. Resist.*, 2025, **3**(1), 28.
26 H. Kong, S. Qin, D. Yan, S. Bhen, T. Zhang, M. Wang, S. Li, A. Mmpomah-Wireko, M. Bai, E. Zhang and J. Cai, *J. Med. Chem.*, 2023, **66**(12), 7756–7771.
27 T. Xu, Z. Xue, X. Li, M. Zhang, R. Yang, S. Qin and Y. Guo, *J. Med. Chem.*, 2025, **68**(7), 7459–7475.
28 Q. Tang, H. Zhang, K. Chandarajoti, Z. Jiao, L. Nie, S. Lv, J. Zuo, W. Zhou and X. Han, *RSC Med. Chem.*, 2024, **22**, 1223–1234.
29 R. Yang, Z. Xue, X. Li, T. Xu, Y. Zhong, S. Hu, S. Qin and Y. G. uo, *Eur. J. Med. Chem.*, 2024, **271**, 116449.
30 R. Yang, L. Cui, T. Xu, Y. Zhong, S. Hu, J. Liu, S. Qin, X. Wang and Y. Guo, *Eur. J. Med. Chem.*, 2024, **279**, 116868.
31 L. Di, *Expert Opin. Drug Discovery*, 2021, **16**(12), 1453–1465.
32 Y. Wang, J. Xiong, F. Xiao, W. Zhang, K. Cheng, J. Rao, B. Niu, X. Tong, N. Qu, R. Zhang, D. Wang, K. Chen, X. Li and M. Zheng, *J. Cheminf.*, 2023, **15**(1), 76.